

# Damage Resistance of a Co-cured Composite Wing Box to Low-Velocity Impact

# 1 Introduction

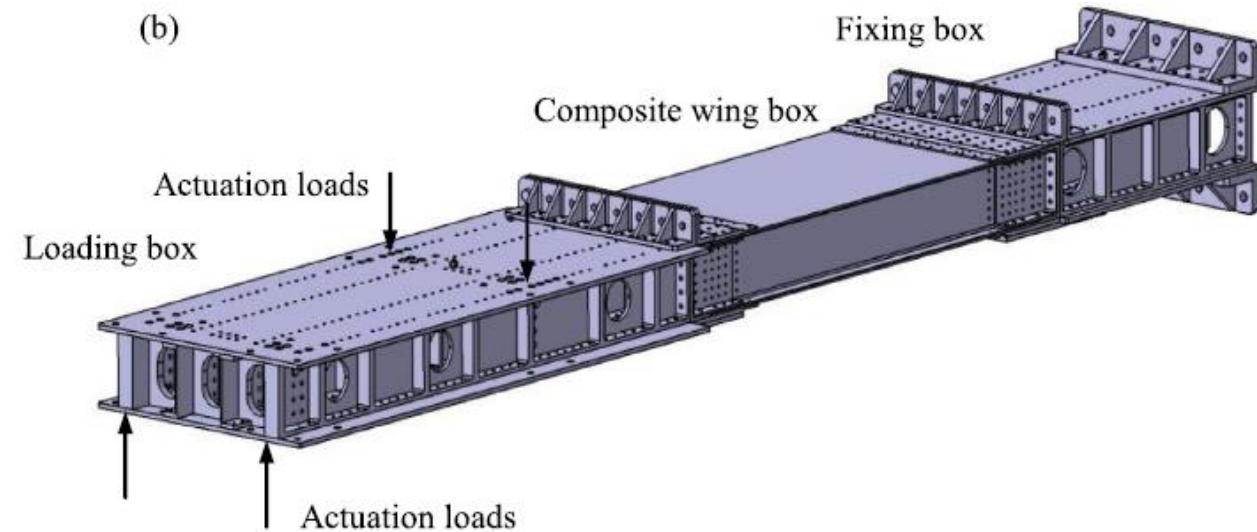
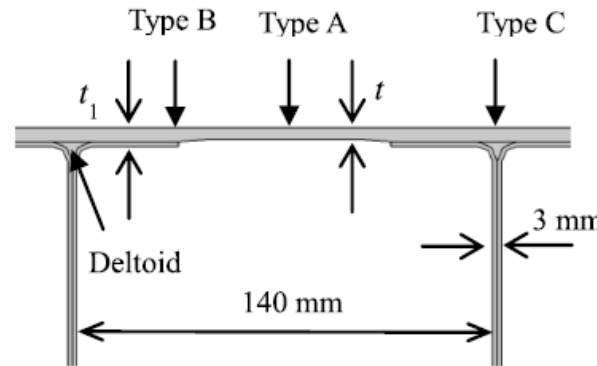
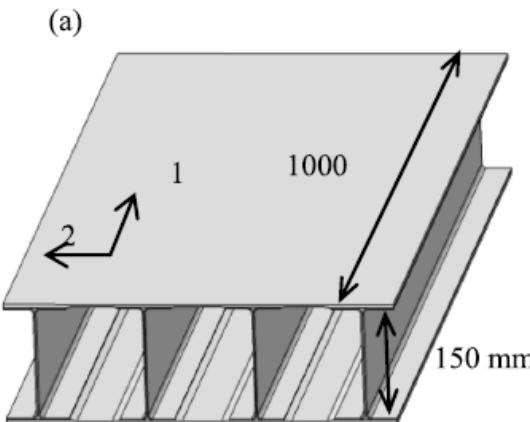
- Composite laminates have poor resistance to low-velocity impact
  - Caused by dropping tools
- Delamination is a serious damage
  - Hard to detect through visual inspection → Causes earlier buckling failure
- Impact on a small specimen
  - Regarded as quasi-static procedure → Contact force and plate response are in phase
  - The spring-mass model for simulating
- Low-velocity impacts were applied to an aircraft wing box fabricated by co-curing its spar and skin

Delamination threshold load (DTL)  
Energy absorbed  
Permanent indentation

Primary parameters for the damage resistance of composite laminates to low-velocity impact

# 2 Composite Wing Boxes & Experiment Setup

- Two wing boxes fabricated using carbon fibre-reinforced plastic composites:
  - First wing box is for the responses of the panel to low-velocity impacts
  - Second one is tested with the static bending load (five typical points) → Effect of the impact damage on structural strength



**Wing Box:** comprises skins and spars.

- Each spar consists of two beams with a channel cross-section.
- The deltoid region is formed by the two beams
- The skin was filled with the fibre bundle.
- Stacking sequence is [45/-45/02/(45/-45)290]s
- The thickness of the skin is 3.76mm
- The skin and the spar were co-cured.
- Three types of sites were subjected to the low-velocity impact:
  - **Type A:** at the bay between the spars
  - **Type B:** at the edge of the flange
  - **Type C:** exactly over the web.

- The wing box was connected to two steel boxes
  - Fixed at its two ends
- Four hydraulic actuators → To exert torsional and bending loading
- A drop tower → To produce the low-velocity impact
- The contact force was measured with the dynamic force sensor.
- The mass of the impactor can be adjusted by adding weights (10.4-5.3kg).



# 3 Results of Impact Tests

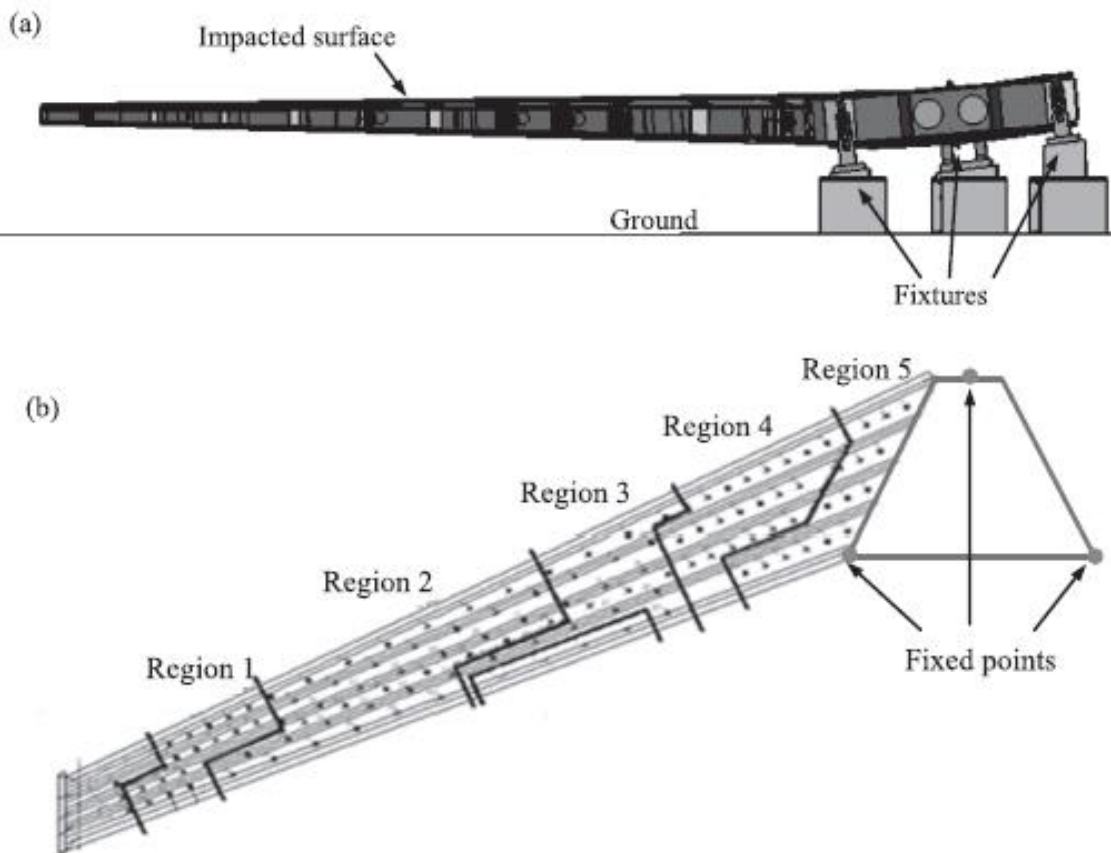


**Table 1**  
Layup parameters of the regions of the composite horizontal tail.

| Regions  | Ply amount | $t/\text{mm}$ | $t_1/\text{mm}$ |
|----------|------------|---------------|-----------------|
| Region 2 | 20         | 3.76          | 6.03            |
| Region 3 | 24         | 4.51          | 7.22            |
| Region 5 | 40         | 7.52          | 3.61            |

Composite horizontal tail: (a) fixtures setup (b) regions subjected to impact

### 3.1 Impact of Type A

- Energy ranging from 10 J to 60 J
- Peak force is lower than DTL of the 15J impact ( $\sim 5290$  N)
- Less than 5290 N → Significant damage does not occur

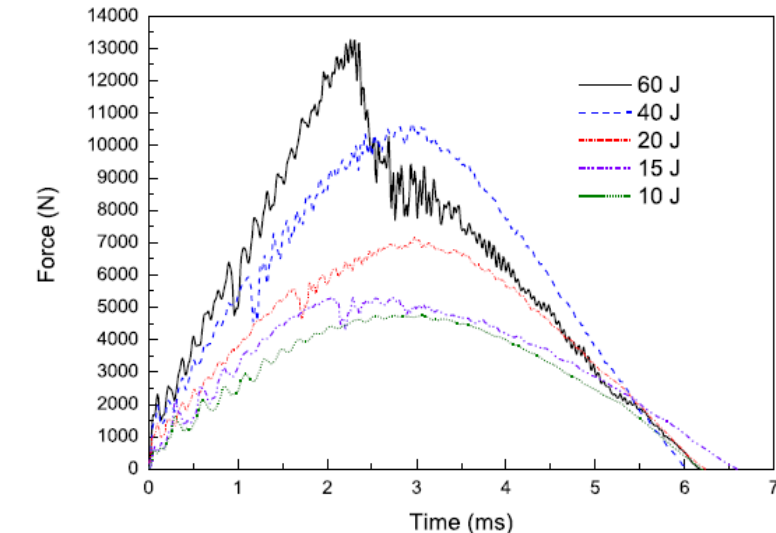


Fig. 4. Contact force histories of the type-A impact on the wing box.

- Sharp drop in each curve for the impact greater than 10 J
- The dramatic load drop at the peak in the 60-J curve :
  - Major portion of the delamination damage.
  - Crushing of the matrix and breakage of fibre at point
  - Significant indentation was then observed

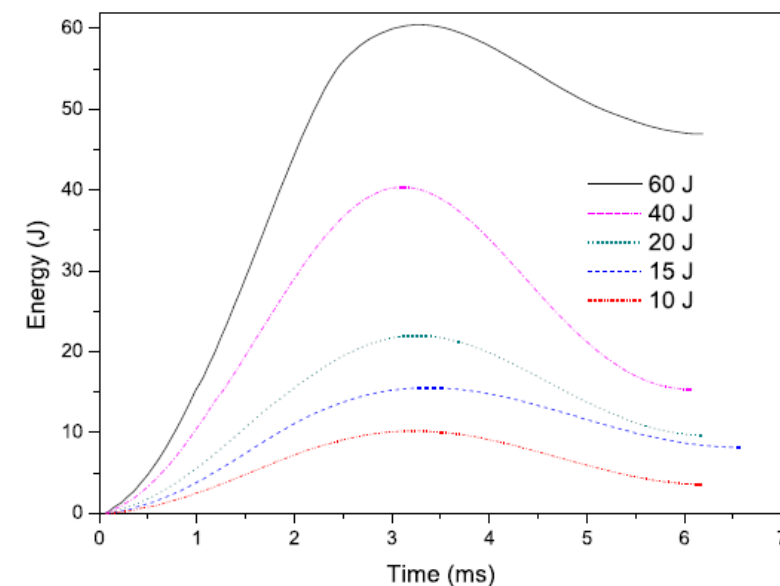


Fig. 7. Time histories of energy absorbed in the type-A impact on the wing box.

### **3.2. Impact of Type B**

- Ranging from 10 J to 65 J
- Average DTL is equal to 6872 N
- A sharp drop appears when impact energy >10 J

### **3.3 Impact of Type C**

- Ranging from 10 J to 60 J
- Secondary bump after the peak in the 40J & 60J
- No sharp drop occurs in the contact force
- The horizontal tail has lower stiffness than wing box → Impact energy was absorbed over structure

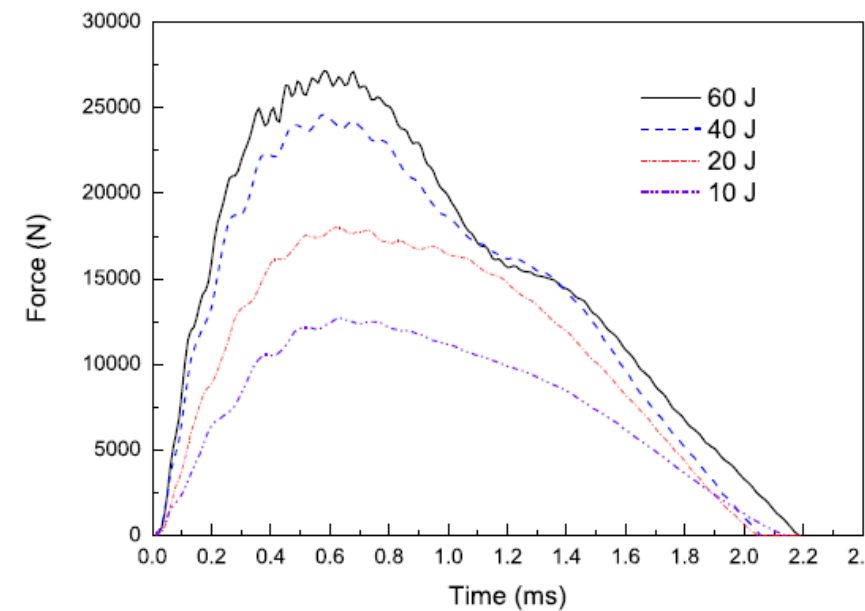
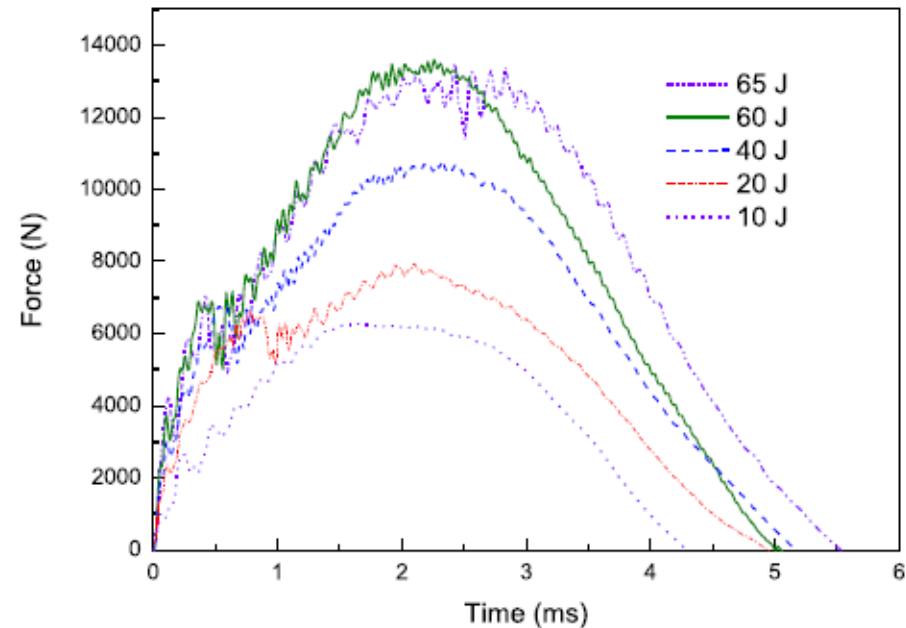


Fig. 14. Contact force histories of the type-C impact on the wing box.

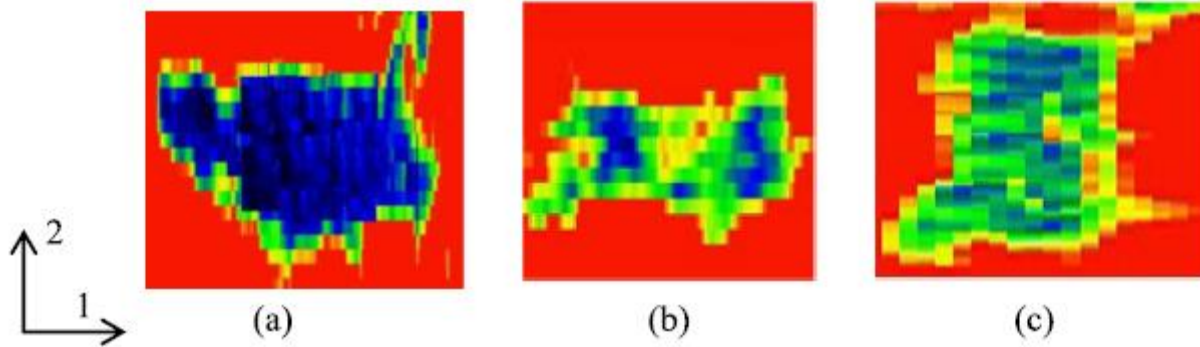


Fig. 5. Ultrasonic C-scans of the delaminations under the 40-J impacts: (a) type A, (b) type B, and (c) type C

**Table 2**  
Dimensions of the damage area of the wing box.

| Impact type | Impact energy (J) | Dimensions of damage area along direction 1 and direction 2 (mm × mm) |
|-------------|-------------------|---|
| A           | 15                | 27.8 × 16.5   |
|             | 20                | 21.0 × 23.3   |
|             | 40                | 38.3 × 27.1   |
|             | 60                | 33.8 × 26.3   |
| B           | 20                | 45.8 × 23.3   |
|             | 40                | 30.8 × 12.8   |
|             | 65                | 40.5 × 18.8   |
| C           | 20                | 9.0 × 7.5   |
|             | 40                | 13.5 × 11.3   |
|             | 60                | 15.0 × 19.5   |

**Table 3**  
DTL prediction for type B for the wing box.

| Impact energy (J) | Experimental DTL for type A (N) | Experimental DTL for type B (N) | Predicted DTL for type B (N) | Prediction error/% |
|-------------------|---------------------------------|---------------------------------|------------------------------|--------------------|
| 65                | -                               | 7059                            | -                            | -                  |
| 60                | 6395                            | 7049                            | 7449                         | 5.7                |
| 40                | 5946                            | 6773                            | 6926                         | 2.3                |
| 20                | 5579                            | 6608                            | 6498                         | 1.7                |
| 15                | 5290                            | -                               | 6162                         | -                  |
| Average           | 5802                            | 6872                            | 6758                         | 1.7                |

### **3.4. Prediction of DTL for Type-B Impact**

- To predict the DTL of type-B location with the experimentally determined DTL of type-A location

### **3.5. The Impact Indentation**

- General visible indentation occurs :
  - at 55 J for the Type-A impact
  - at 65 J for the Type-B impact.
    - Indentation is barely visible under 60 J
    - But cracks are generated on the surface
  - No indentation for the type-C impact
    - But a scar due to the high contact force

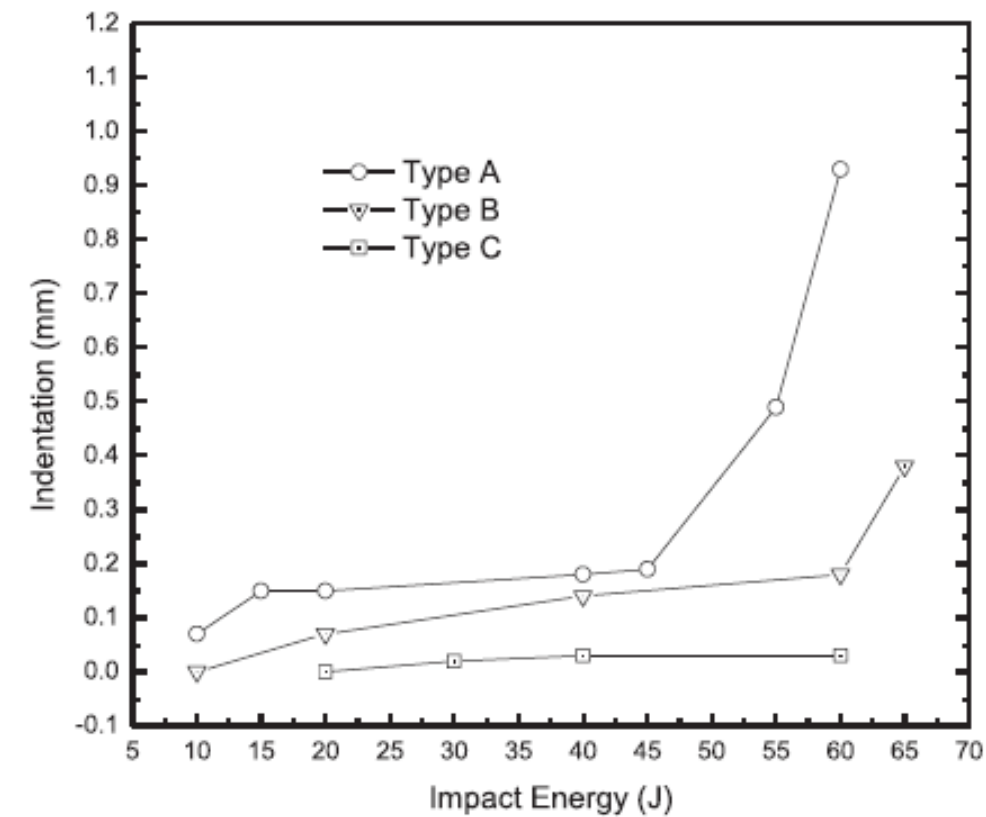


**Fig. 19.** Comparison of indentations of impacts on the wing box.

# 4 Ultimate Load Test After the Low-Velocity Impact

- A limited bending moment of  $0.5 \times 10^5$  Nm is applied to second wing box without damage first.
- Five impact tests of 60 J is conducted on the upper surface of the wing box.
- Bending is applied to the wing box with impact damage
  - Breaks along the line at the bending moment of  $1.1 \times 10^5$  Nm.
- Impact damage does not weaken the wing box to bear the limited load.
- The critical load of buckling of wing box is  $\sim 0.8 \times 10^5$  Nm.

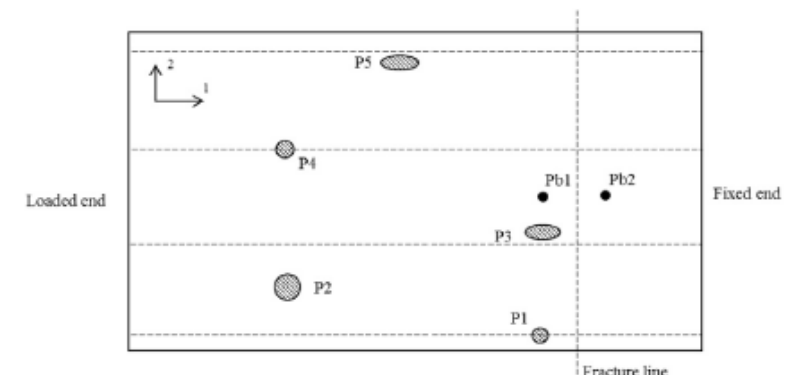


Fig. 20. Impact points and delamination regions of the wing box.

# 5 Conclusion

This study investigated:

- the contact force, energy absorption, delamination, and indentation due to low-velocity impact on the panel of a composite wing box.
- The characteristics of Type-A impact are consistent with the standard test on the specimen.
- The sharp drop in the F–t curve for the Type-A & Type-B impacts → Causes the delamination.
- Very high contact force is generated by the Type-C impact
  - Size of the delamination area is small
  - Shallow indentation is observed.

- The energy absorption is high for the impacts on the horizontal tail.
- The proposed model is effective in predicting the DTL of the Type-B impact with the experimentally determined DTL of Type-A
- To investigate the behavior of the damaged region under compressive load, impact damage is applied to the wing box.

- The wing box was broken after it began to buckle.
  - The strain response at the other impact points exhibited good damage resistance to Type-B and Type-C impacts.
- The failure position is close to the supporting end
  - Rather than the impact point where the delamination propagation occurs.
  - The impact point should be located in this region when investigating the effects of the impact damage on ultimate load of composite panel.

# Co-Curing Process Combining Resin Film Infusion with Prepreg and Co-cured Interlaminar Properties of Carbon Fiber Composites

# 1 Introduction

- The carbon fiber/epoxy resin matrix composite laminates were fabricated using a co-curing process combining resin film infusion (RFI) process with prepreg-autoclave process (co-resin film infusion)
  - Low-cost for advanced composite structure
  - High mechanical performance
- Co-cured liquid composite molding (co-LCM) is an integral forming technique for combining liquid molding process with prepreg curing process.
  - The co-LCM technology improves the processability of complex structure
  - Achieves the purposes of time-saving and cost-saving by means of reducing fasteners, assembling procedures and simplifying mold.

- This papers:
  - Develops co-LCM in co-RTM → To fabricate aircraft structures
  - Proposes a new idea of co-RFI
    - Co-cures RFI part with prepreg stack simultaneously for taking advantages of cost-effectiveness of RFI and high properties of unidirectional prepreg.
- Two kinds of resins are used during co-LCM process:
  - Resin in prepreg stack
  - Resin for infusion
- Co-cured laminate was compared with RFI laminate and prepreg laminate:
  - Processing quality
  - Mode I and Mode II interlaminar fracture toughness

# 2 Experiment

## **2.1 Materials:**

- A kind of epoxy resin film (MTM 44-1)
- T700SC (12k tow) unidirectional carbon fiber (for RFI process)
- HTS 5631 (12k tow)/MTM 44-1 unidirectional prepreg (for this study)
- An epoxy tackifier (for binding CFW-200 fabrics in RFI process and powder form)

## **2.2 Composite Manufacturing:**

### **Prepreg-autoclave process:**

- MTM 44-1 is cured with teflon film (To form pre-crack)
- Recommended cure cycle was applied in autoclave. Vacuum is applied.
- Temperature is increased:
  - Room temperature to 180°C at 2°C/min and maintained at 180°C for 2 h.

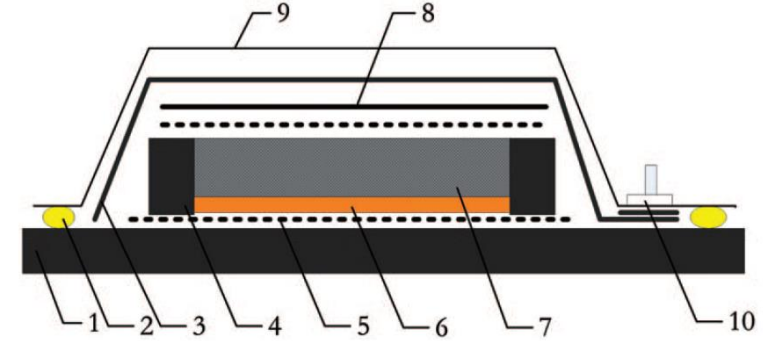


**Figure 1.** Schematic of the bagging procedure in RFI process.

1 – steel plate, 2 – sealant, 3 – breather, 4 – dam, 5 – resin film, 6 – fiber fabric, 7 – release film, 8 – vacuum bag, 9 – vacuum valve.

## RFI process:

- The stack contains 20 layers of CFW-200 (in 0 direction) and nine layers of resin film
  - The release film was used → To ensure entrapped air to be released.
  - Teflon film was placed in mid of the fiber stack.
1. Heat from 25°C to 180°C at 2°C/min and hold at 180°C for 120 min.  
(Recommended by manufacturer, **Process A**)
  2. Heat from 25°C to 130°C at 2°C/min and hold at 130°C for 30 min. Then, increase to 180°C at 2°C/min for 120 min. (**Process B**)
  3. Disperse 8wt% tackifier on the surface of CFW-200 and maintain 5 min at 80°C. Then, the same cure cycle as Process B. (**Process C**)

## Co-RFI process:

- 16 MTM 44-1 prepreg layers, 10 CFW-200 fabric plies and five layers of resin film (in 0 direction)
- Two kinds of lay-up types: Prepreg layers at the top of stack (prepreg/RFI) , Prepreg layers on bottom of stack (RFI/prepreg)
- Manufactured in an autoclave using Processes A, B and C.

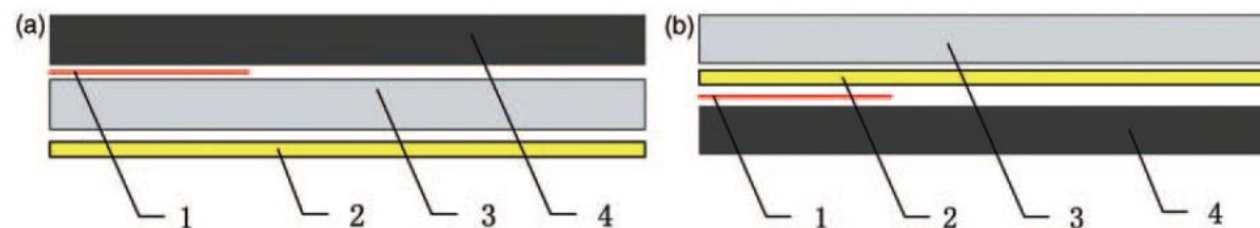


**Figure 3.** Schematic of two kinds of lay-up types: (a) prepreg/RFI stack and (b) RFI/prepreg stack.  
1 – Teflon film, 2 – five layers of resin film, 3 – 10 carbon fiber fabric plies, 4 – 16 prepreg layers.

# 3 Testing

## 3.1 Resin Viscosity

- Using a Gemini rheometer

## 3.2 Mode I Interlaminar Fracture Toughness

- Using the double cantilever beam (DCB) specimen
- DCB specimen Width = 25mm and Length = 150mm
- The critical  $G_{IC}$  is calculated as average of  $G_{IC}$  values at beginning of delamination

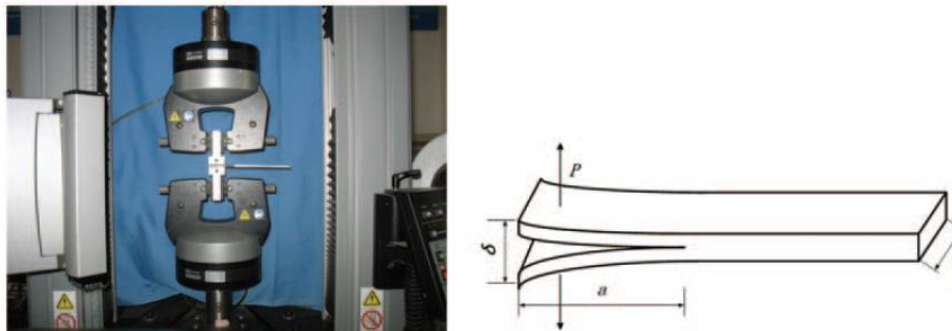


**Figure 4.** Schematic of DCB testing:  $a$  = crack length,  $p$  = Load,  $\delta$  = displacement.  
DCB: double cantilever beam.

### **3.3 Mode II Interlaminar Fracture Toughness**

- Using the end notched flexure (ENF) specimen.
- The ENF specimen; Width = 25mm and Length = 140mm
- Initial  $G_{IC}$  is calculated as average of  $G_{IC}$  values using the crack initiation loading for each specimen group

### **3.4 Processing Quality Observation**

- Observation by
  - Optical micrograph → To observe defects inside laminates
  - Laminate thickness
- Using scanning electron microscopy → To observe crack surface of samples

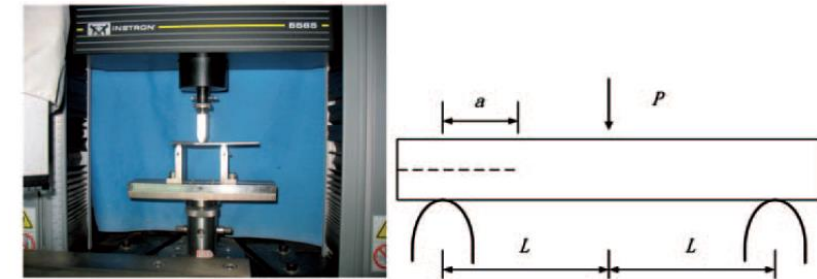


**Figure 6.** Schematic of ENF testing:  $a$  = the effective crack length,  $p$  = load,  $L$  = a half of the span length.  
ENF: end notched flexure.

# 4 Results and Discussion

## 4.1 Processing Quality of Co-Curing Process

- Quality of prepreg laminate is perfect without void and the prepreg/RFI laminate cured by Process A gives the maximum value (about 0.86%)
- Void contents in co-cured interface are higher than integral laminates (especially for prepreg/RFI laminates)
- Isothermal dwell (in Process B) has great influence on decrease of voids at the laminate
- Addition of the tackifier almost has no influence on the flow and infiltration of the matrix resin
  - But makes the resin more redundant than the laminates without tackifier.

**Table 3.** The void content of different laminates.

|                      | Void content (%) |                 |                 |
|----------------------|------------------|-----------------|-----------------|
|                      | Process A        | Process B       | Process C       |
| RFI laminate         | 0.03             | 0.02            | 0.01            |
| RFI/prepreg laminate | 0.03             | 0.01            | 0.01            |
| Prepreg/RFI laminate | $0.86 \pm 0.03$  | $0.63 \pm 0.02$ | $0.59 \pm 0.01$ |
| Prepreg laminate     | 0                | —               | —               |

## 4.2 Evaluation Of Co-RFI Laminate Interface

- $G_{IC}$  of RFI/prepreg laminate is 192 J/m<sup>2</sup>.
- $G_{IC}$  of prepreg/RFI is 190 J/m<sup>2</sup>.
- Prepreg laminate has the maximum critical  $G_{IC}$ (222 J/m<sup>2</sup>).
- RFI processed laminate gives the minimum  $G_{IC}$ (168 J/m<sup>2</sup>).
- The cracks in the prepreg laminate runs along the centerline without deflection.

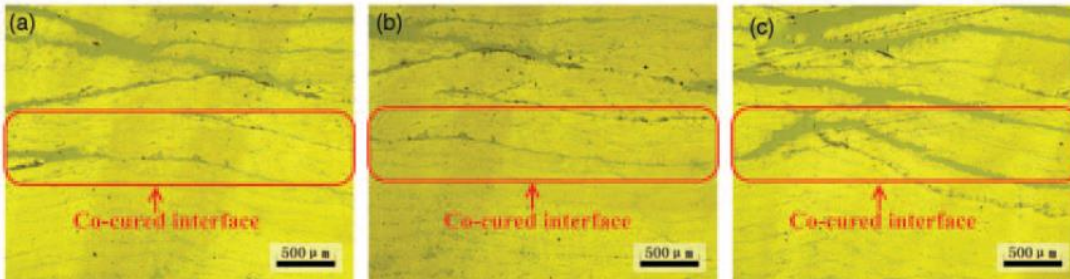


**Figure 10.** Micrographs of RFI/prepreg laminates cured by: (a) Process A, (b) Process B and (c) Process C.  
RFI: resin film infusion.

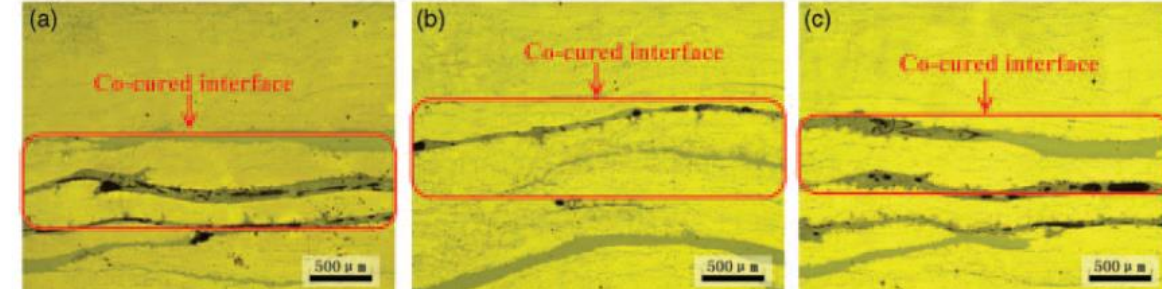


**Figure 11.** Micrographs of prepreg/RFI laminates cured by: (a) Process A, (b) Process B and (c) Process C.

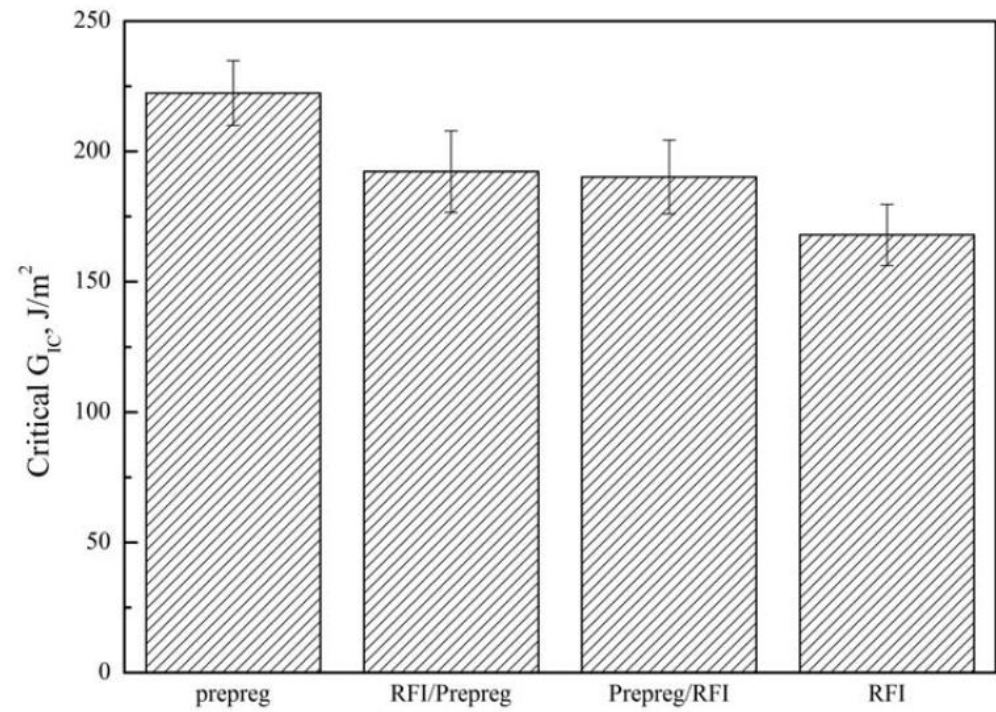


**Figure 13.** The critical  $G_{IC}$  values of different laminates fabricated using Process A.

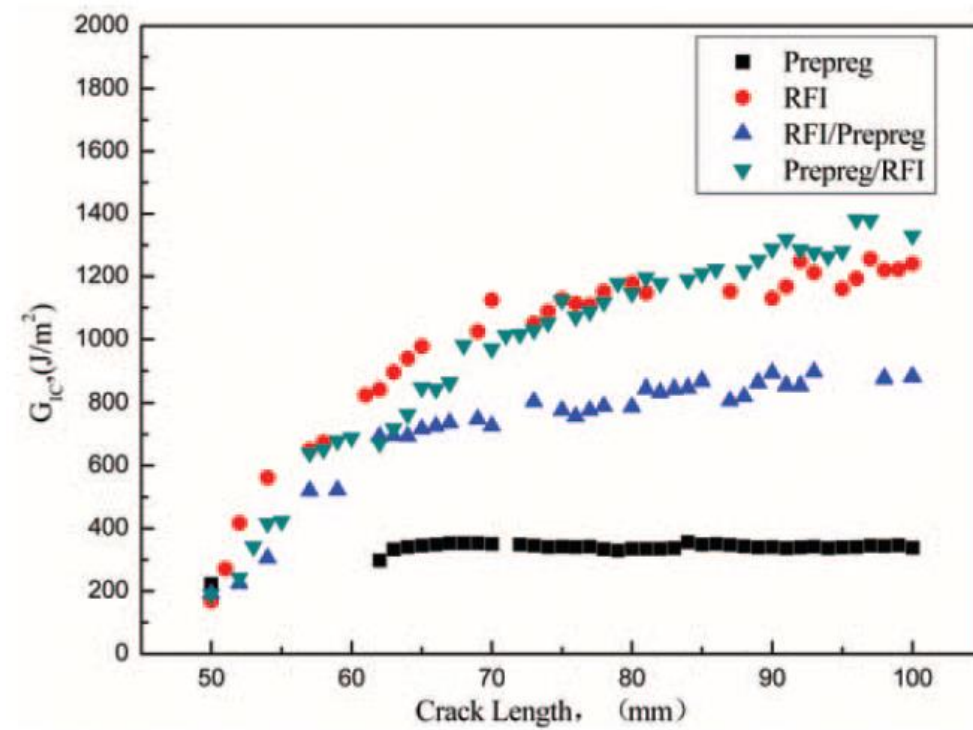


**Figure 14.** Mode I delamination resistance curves (R-curves) of laminates cured by Process A.

#### **4.3 Influence Of Isothermal Dwell And Tackifier On The Interlaminar Properties**

- The laminates co-cured under Processes B and C are tested through the Mode I and Mode II interlaminar fracture toughness
- The effects of the isothermal dwell and the tackifier on the interlaminar properties of co-cured interface are evaluated.

## Influence Of Isothermal Dwell:

- Initial  $G_{IC}$  of co-RFI laminates fabricated using Process A and B.
- Significant increase in the initial  $G_{IC}$  for the composite laminates cured by Process B, compared to Process A.

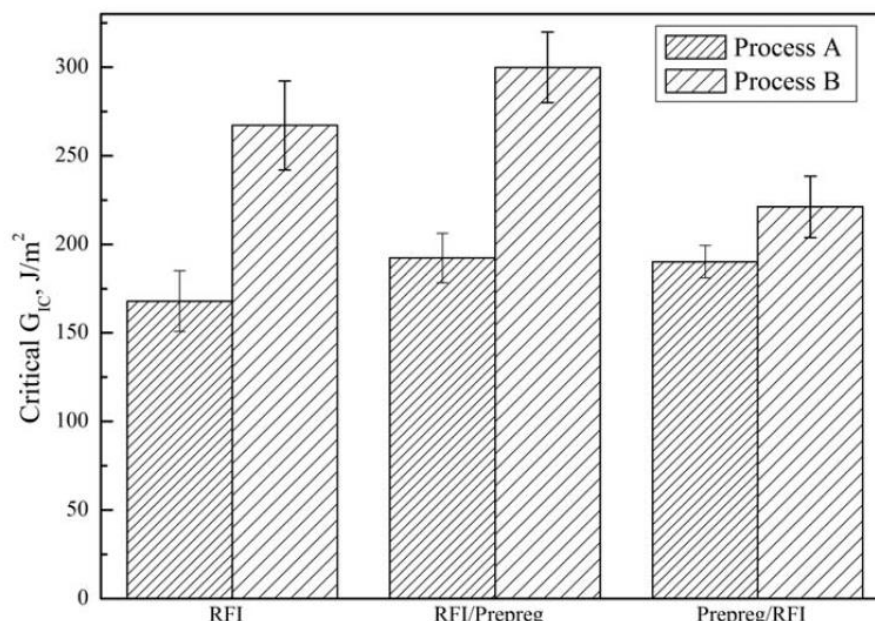


Figure 17. The initial  $G_{IC}$  values of laminates cured by Process A and Process B.

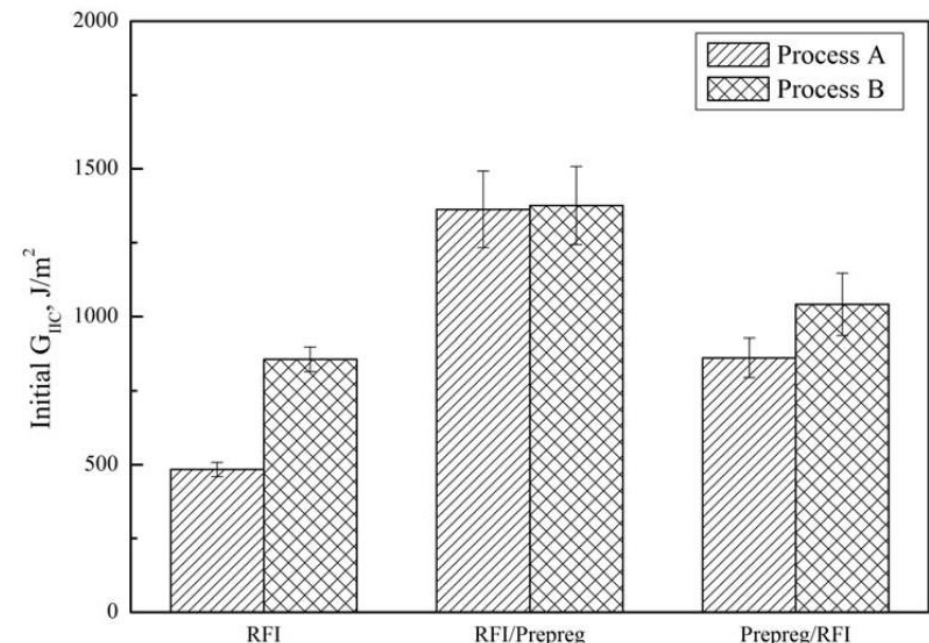


Figure 19. The initial  $G_{IIC}$  values of laminates cured by Process A and Process B.

## Influence Of Tackifier:

- Tackifier has effect on the interlaminar fracture toughness of laminates.
- Initial  $G_{IC}$  of RFI laminate with tackifier is improved compared with the RFI without tackifier
- But initial  $G_{IC}$  values of co-RFI laminates with tackifier decrease in contrast with co-RFI without tackifier.

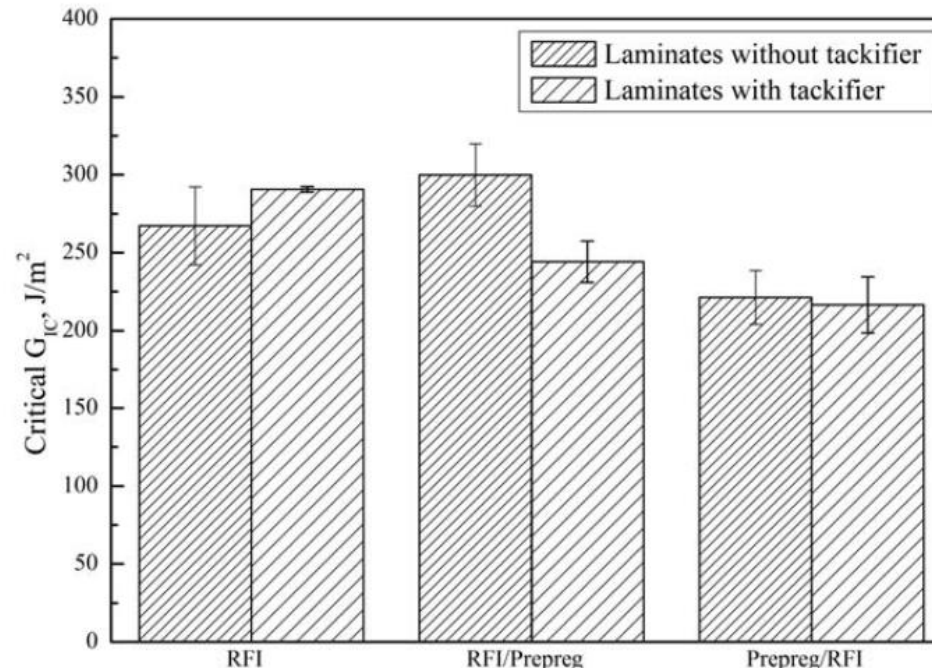


Figure 20. The critical  $G_{IC}$  values of laminates cured by Process B and Process C.

**Table 5.** The initial  $G_{IC}$  values of laminates cured by Processes A, B and C.

|                      | The initial $G_{IC}$ values |                |                |
|----------------------|-----------------------------|----------------|----------------|
|                      | Process A                   | Process B      | Process C      |
| RFI laminate         | 167.96 ± 17.09              | 267.17 ± 25.09 | 290.59 ± 1.84  |
| RFI/prepreg laminate | 192.28 ± 14.01              | 299.87 ± 19.95 | 244.15 ± 13.21 |
| Prepreg/RFI laminate | 190.18 ± 9.10               | 221.17 ± 17.35 | 216.44 ± 17.93 |

RFI: resin film infusion.

**Table 6.** The initial  $G_{IIC}$  values of laminates cured by Process A, B and C.

|                      | The initial $G_{IIC}$ values |                   |                  |
|----------------------|------------------------------|-------------------|------------------|
|                      | Process A                    | Process B         | Process C        |
| RFI laminate         | 547.96 ± 21.58               | 1159.90 ± 53.34   | 1838.77 ± 72.05  |
| RFI/prepreg laminate | 1414.77 ± 78.15              | 2031.17 ± 135.70  | 2553.02 ± 109.44 |
| Prepreg/RFI laminate | 1155.205 ± 46.37             | 1776.62 ± 169.335 | 984.44 ± 126.98  |

RFI: resin film infusion.

# 5 Conclusion

- Optical photographs of the laminates cured by co-RFI shows
  - Matrix-rich regions and voids mostly exist in RFI part and the interlaminar interface between the prepreg part and RFI part.
  - The matrix-rich regions and voids at the co-cured interface reduce the interlaminar properties of the co-RFI laminates, causing a lower delamination resistance
- Isothermal dwell before curing process has a great influence on the interlaminar fracture toughness of co-RFI laminates
  - Improves the interlaminar fracture toughness → Due to low resin viscosity and infusion time for improving the impregnation degree of the fiber preform.

- Epoxy tackifier is an important factor to make the resin redundant
  - Enlarges the matrix-rich region at the co-cured interface, and changes the interlaminar fracture toughness.

# An Analytical Model For B-Stage Joining and Co-curing of Carbon Fibre Epoxy Composites

# 1 Introduction

- Paper develops cure kinetic models
    - To describe the B-stage curing
    - Co-curing assembly of **carbon fibre reinforced thermosetting polymer (CFRP)** composites
  - **Problem** of using CFRP materials:
    - Inefficient joining procedures
    - Strict certification standards
  - **The solution:**
    - To partially cure two subassemblies, combine them and complete the cure cycle for both
- Lost in efficiency

- Co-cured joints also provide higher fracture toughness and joint strength than co-bonded joints
- Cure kinetic modelling of thermoset resins is widely used
- Most works focus on wide temperature ranges, model optimisation for a wide range of degree of cure
  - Such models are insufficient for B-Stage curing and co-curing (due to variance in a few degrees )
- A new approach is proposed to describe B-Stage curing and co-curing assembly by using the developed kinetic model

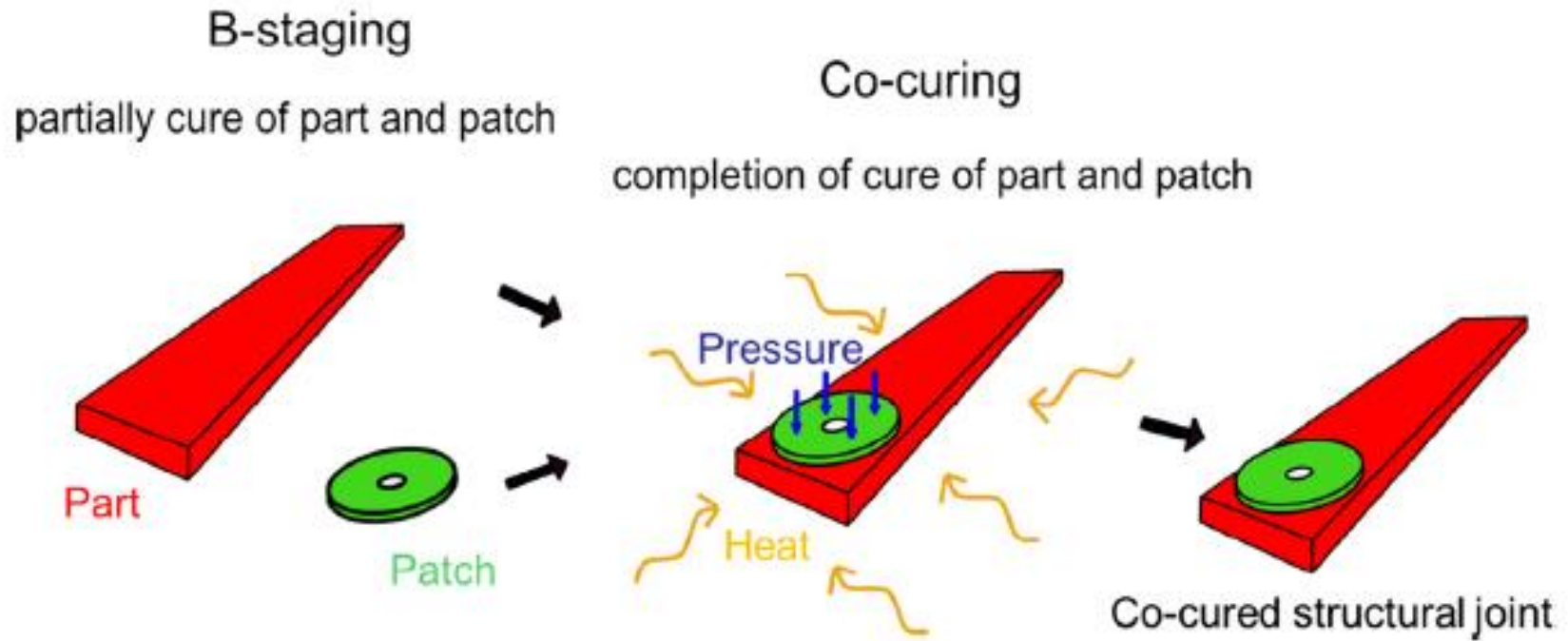


**Fig. 1.** Shows the concept of patch reinforcement of a structural part via co-curing of B-stage cured components. (For interpretation of the references to colour in this figure legend, the reader is referred to the web version of this article.)

## 2 Materials

- **Resin:** HexFlow RTM6
- **CFRP parts:** Manufactured by a RTM process
- **Reinforcing CFRP patches:** Manufactured from thin ply material
- **Nylon peel:** To prepare surfaces for co-curing

# 3 Experimental

- The differential scanning calorimetry (DSC) measurements were made

## 3.1 Resin Cure Kinetics

- Isothermal and dynamic DSC measurements of the uncured resin were made as reference data for the analytical modelling

## 3.2 B-stage Degree Of Cure

- The resin was heated to 80 C for one hour
- Transferred to a plate heated vacuum oven
- Degassed to 20 kPa for five minutes
- Circa 0.8 kPa vacuum pressure for a further 25 min

- The CFRP parts were cured at 400 kPa for varying times at 160°C
- Completely cured parts were cured at 180°C for 90 minutes in the RTM tool
- The B-stage cured CFRP parts were cured at 160°C in the RTM tool

### **3.4 Co-Curing Of the CFRP Part and Patch**

- The CFRP patch and CFRP part were prepared by first removing peel plies (for adhesive)

## 4. Models and Methodology

- The curing reaction is applied using DSC of the pure resin at different temperatures and heating rates .
- Kinetics of the curing reaction of the resin are investigated.

### **4.1. Model For Evolution Of T<sub>g</sub> and Resin Cure Kinetics**

- DiBenedetto model is used to describe T<sub>g</sub> as a function of  $\alpha$  (degree of cure).

### **4.2. B-Stage Curing Cycle Of the CFRP Part and Patch**

- 

### **4.3. Co-Curing Cycle Of the CFRP Part and Patch**

-

# 5 Result

- **5.1 DSC Measurements**

- **5.2 Comparison Of The Measured And Predicted B-Stage**

### **5.3 Co-curing Of The CFRP Part And Patch**

-

## **5.4 Discussion**

# 6 Conclusion

- This work demonstrated an approach for using the developed kinetic model to describe the B-stage curing and co-curing assembly of local reinforcement.
- Described methodology to locally reinforce a partially cured structure has proved to be possible and presents techniques that are readily scalable, and cost effective.
- **Biggest challenge** for industrialisation is to the narrow window for the free standing cure of the CFRP part presented by the RTM6 resin system.